Article

Novel Bionanocellulose/κ-Carrageenan Composites for Tissue Engineering

Izabela Cielecka [1,*], Marcin Szustak [1], Edyta Gendaszewska-Darmach [1] , Halina Kalinowska [1], Małgorzata Ryngajłło [1] , Waldemar Maniukiewicz [2] and Stanisław Bielecki [1]

1   Institute of Technical Biochemistry, Lodz University of Technology, Stefanowskiego 4/10, 90-924 Lodz, Poland; marcin.szustak@edu.p.lodz.pl (M.S.); edyta.gendaszewska-darmach@p.lodz.pl (E.G.-D.); halina.kalinowska@p.lodz.pl (H.K.); malgorzata.ryngajllo@p.lodz.pl (M.R.); stanislaw.bielecki@p.lodz.pl (S.B.)

2   Institute of General and Ecological Chemistry, Lodz University of Technology, Żeromskiego 116, 90-924 Lodz, Poland; waldemar.maniukiewicz@p.lodz.pl

*   Correspondence: izabela.cielecka@edu.p.lodz.pl; Tel.: +48-42-631-3367

check for updates

Featured Application: Bionanocellulose/κ-carrageenan composites developed within this study meet the specific tissue engineering requirements, including high tensile and compression strength, water holding capacity, and water retention ratio, suitable swelling properties as well as the positive effect on cell differentiation. As the key properties of these composites may be easily modified during their fabrication, the established procedure may lead to the production of customized scaffolds.

Abstract: In this work, novel bacterial cellulose/κ-carrageenan (BNC/κ-Car) composites, being potential scaffolds for tissue engineering (TE), and outperforming the two polymers when used as scaffolds separately, were for the first time obtained using an in situ method, based on the stationary culture of bacteria *Komagateibacter xylinus* E25. The composites were compared with native BNC in terms of the morphology of fibers, chemical composition, crystallinity, tensile and compression strength, water holding capacity, water retention ratio and swelling properties. Murine chondrogenic ATDC5 cells were applied to assess the utility of the BNC/κ-Car composites as potential scaffolds. The impact of the composites on the cells viability, chondrogenic differentiation, and expression patterns of *Col1α1*, *Col2α1*, *Runx2*, and *Sox9*, which are indicative of ATDC5 chondrogenic differentiation, was determined. None of the composites obtained in this study caused the chondrocyte hypertrophy. All of them supported the differentiation of ATDC5 cells to more chondrogenic phenotype.

Keywords: bacterial cellulose; κ-carrageenan; composite; tissue engineering; chondrocytes

1. Introduction

Articular cartilage tissue consists of chondrocytes growing in an extracellular matrix (ECM), which is responsible for the adhesion and differentiation of cells and cell-to-cell communication. The principal components of ECM are certain fibrous proteins; e.g., type II collagen, proteoglycans, hyaluronic acid, and chondroitin sulfate [1]. Articular cartilage protects the bone ends from friction and compressive loads. The injuries and articular diseases are frequent and may cause pain, arthrodesis, and joint arthoplasty. Due to the limited regenerative capacity of cartilage, tissue repair methods have been sought for. Traditionally, autografts and allografts are used to treat these lesions. However, the donor cartilage tissue is not only available in insufficient amounts but also may induce an immune

response, leading to the implant's failure. Tissue engineering (TE) is the promising alternative of cartilage defects treatment. However, its success depends on four key factors such as cells, mechanical environment, growth factors, and scaffolds. An ideal scaffold must fulfill a wide range of criteria, such as biocompatibility, porosity and suitable 3D structure, high water absorption capacity, and high mechanical strength. Furthermore, it has to promote the proliferation of chondrocytes and ensure the diffusion of nutrients, active substances and growth factors. Over the last years, various materials have been studied as potential matrices for TE, being able to mimic the ECM. They are classified as either synthetic (polylactic acid, polyethylene glycol) or natural that are based on proteins (collagen, fibrin, silk) and polysaccharides (hyaluronic acid, chitosan, alginate, cellulose) [2,3].

Like plant cellulose, bacterial bionanocellulose (BNC) is a linear polymer composed of β-1,4-linked D-glucopyranose residues. It is produced as an exopolysaccharide having a form of the three-dimensional network of nano-sized fibers by various species of bacteria, such as those of the genera *Komagataeibacter*, *Agrobacterium*, *Rhizobium*, and *Sarcina* [4]. BNC exhibits many desirable and unique properties such as biocompatibility [5], high mechanical strength, and water holding capacity up to 100 times its dry mass [6] as well as high crystallinity and porosity. Biocompatibility of BNC-based products makes them suitable for numerous biomedical applications, such as wound dressings [7,8], artificial vessels [9,10], cornea replacements [11], drug delivery systems [12,13] and scaffolds for tissue engineering [14].

The interactions of the biomaterial with surrounding cells depend on the proper distribution of functional groups in three-dimensional space [15]. The native BNC-based scaffolds promote neither the excellent cell adhesion nor growth because cellulose is biologically inactive, mainly due to its neutral charge [16,17]. Therefore, there is a need to modulate the intrinsic properties that may be particularly beneficial in the biomedical application by introducing for instance a negative charge promoting interactions with proteins in the extracellular matrix [18]. For this purpose, we created a composite of bacterial nanocellulose with sulfate groups-rich κ-carrageenan (κ-Car). κ-Car, widely used in the food industry due to its excellent gelling capacity, belongs to the family of linear polysaccharides extracted from red seaweeds, *Rodophyta*. Carrageenans, built from 3-linked β-D-galactopyranose and 4-linked α-D-galactopyranose or 4-linked 3,6-anhydro-α-D-galactopyranose units [19], are divided into the iota (ι-), kappa (κ-) and lambda (λ-) forms, and their mu (μ-) and nu (ν-) precursors [20,21]. The classification is based on a number and position of sulfate groups on the repeating disaccharide units. κ-Car, potentially used as a pharmaceutical material due to its good biocompatibility and low toxicity, contains one sulfate group on the C4 of β-D-galactopyranose residue [22]. Upon cooling it forms gels in the presence of K^+, Na^+ or Ca^{2+} ions via aggregation of double helices [23]. Due to its gelation ability, high water absorption capacity, and an ester sulfate content of 25–30%, κ-Car has a great applicability in drug delivery systems [24,25], for cells encapsulation [26] and as a wound dressing [27]. The composition imitating glycosaminoglycans makes it a potential scaffold for tissue engineering of cartilage. Nevertheless, there are same inconveniences when using κ-Car as an independent scaffold, such as limited swelling properties, unsatisfactory mechanical strength, or the fragility of created gels [28].

The proposed BNC/κ-Car composites in this work enable to overcome the limitations of the two polymers when used separately. To the best of our knowledge, this is the first report on the production of bacterial cellulose/κ-carrageenan composites using an in situ method.

In this paper, we report the preparation of new BNC/κ-carrageenan composites and the evaluation of their properties. The morphology of fibers, chemical composition, crystallinity, tensile, and compression strength, water holding capacity, water retention ratio and swelling properties were examined and compared with those of pure BNC. Furthermore, we examined the influence of BNC/κ-carrageenan composites on chondrogenic differentiation as a goal of cartilage tissue engineering. To evaluate the utility of the BNC/κ-Car composites as potential scaffolds for TE, we applied murine chondrogenic ATDC5 cells that represent a chondroprogenitor clone and assessed

the impact of the composites on their viability as well as the specific expression patterns of *Col1α1*, *Col2α1*, *Runx2*, and *Sox9*, which are indicative of ATDC5 chondrogenic differentiation [29].

2. Materials and Methods

2.1. Microbial Strains

Komagataeibacter xylinus E25 strain used in this study was derived from the Institute of Technical Biochemistry (Lodz University of Technology) collection. The strain belongs to BOWIL Biotech Ltd., Poland.

2.2. Culture Media

K. xylinus E25 strain was cultivated under stationary conditions in a Schramm-Hestrin (SH) medium containing glucose (20 g/L), yeast extract (5.0 g/L), peptone (5.0 g/L), $MgSO_4 \cdot 7H_2O$ (0.5 g/L), anhydrous Na_2HPO_4 (2.7 g/L) and citric acid (1.15 g/L), dissolved in distilled water. The pH of the culture medium was adjusted to 5.7 using 0.1 M acetic acid before autoclaving at 121 °C for 20 min.

2.3. Preparation of BNC, κ-Car and BNC/κ-Car Composites

K. xylinus E25 strain was activated by cultivation in the SH medium at 30 °C for 3 days and used as an inoculum. The medium was supplemented with ethanol (1% (*v/v*)) directly before the inoculation with bacterial pre-culture (5% (*v/v*)). BNC membranes and BNC/κ-Car composites were obtained in stationary conditions at the temperature of 30 °C after 7-day culture. The composites were prepared using two in situ methods. The first method was based on supplementation of the SH medium with κ-Car (final concentrations of 2, 5 and 8 g/L) before the medium sterilization that yielded the composites BNC/κ-Car$_{0.2}$, BNC/κ-Car$_{0.5}$, and BNC/κ-Car$_{0.8}$, respectively. The composites with higher content of κ-Car (BNC/κ-Car$_{2.0}$, BNC/κ-Car$_{4.0}$, and BNC/κ-Car$_{6.0}$) were obtained using the two-step method. In the first step, the SH medium was supplemented with κ-Car (2 g/L) and sterilized (121 °C for 20 min). After cooling, additional portions of sterile κ-Car were added to obtain the final concentrations of 20, 40 and 60 g/L (the composites obtained are referred to as BNC/κ-Car$_{2.0}$, BNC/κ-Car$_{4.0}$ and BNC/κ-Car$_{6.0}$, respectively).

The purification steps of the obtained membranes included rinsing with tap water until flushing out of the remaining medium, 24 h washing with 1% (*w/v*) sodium hydroxide for bacterial cells removal, and subsequent immersing in 1% (*v/v*) acetic acid and then in distilled water for pH neutralization. Purified cellulose membranes were packed and sterilized by autoclaving at 121 °C and stored at 4 °C before further analytical steps.

κ-Car gels were prepared for Fourier-transform infrared spectroscopy (FTIR) analysis and cell viability study. κ-Car was dissolved in 0.1 M $CaCl_2$ by autoclaving (121 °C for 20 min) to obtain solution with concentrations of 2 and 4 g/L, which were immediately transferred into a 96-well plate (1 mL per well), under sterile conditions. Upon cooling κ-Car formed round-shaped pieces of gel (κ-Car$_{0.2}$ and κ-Car$_{0.4}$, respectively), which were freeze-dried (an Alpha 1–2 LD plus lyophilizer, Christ, Germany) and stored in desiccators before using.

2.4. Characterization of BNC/κ-Car Composites

2.4.1. Scanning Electron Microscopy (SEM)

SEM was applied for visual inspection of BNC/κ-Car composites. Freeze-dried samples of the composites were sputter coated with gold layer and observed using a FEI QUANTA 250 FEG microscope (Thermo Fischer Scientific, Waltham, MA, USA) (HV 2 kV, magnification 40,000×). Fibers thickness was evaluated on the basis on SEM images using the Makroaufmassprogramm software. Histograms were drown using the R (v. 3.4.1) software.

2.4.2. Fourier-Transform Infrared Spectroscopy

The incorporation of κ-Car into BNC membranes was evaluated with the FT-IR in an attenuated total reflectance mode (ATR) using a Nicolet 6700 FT-IR (Thermo Fischer Scientific, Waltham, MA, USA). The spectra were recorded over the range from 4000 to 650 cm^{-1} by the accumulation of 200 scans, with a spectral resolution of 4 cm^{-1}.

2.4.3. X-ray Diffractometry

Room temperature powder X-ray diffraction patterns were collected using a PANalytical X'Pert Pro MPD diffractometer (Malvern Panalytical Ltd., Royston, UK) with the Bragg–Brentano reflection geometry and the graphite monochromated Cu-K$_\alpha$ radiation. All data were collected in the 2θ range 5–60° with a step of 0.0167° and an exposure per step of 30 s. The samples were spun during data collection to minimize preferred orientation effects. A PANalytical X'Celerator detector based on the Real Time Multiple Strip technology and simultaneously measuring intensities in the 2θ range of 2.122° was used.

The crystallinity index was calculated as the ratio of the integral intensity under all crystalline peaks to the sum of integral intensity under the crystalline peaks and amorphous halo [30] using the WAXFIT program [31]. Each diffraction curve was analyzed by the creation of a theoretical function best fitted to the experimental curve, according to the hybrid optimization procedure, which combines a genetic algorithm with a modified Rosenbrock optimization method. A linear combination of the Gauss and Lorentz profiles was used to construct the theoretical function approximating crystalline peaks and an amorphous halo. As a result of fitting, all the parameters of the component functions were determined.

2.4.4. Mechanical Strength

BNC/κ-Car composites were examined for tensile and compression strength. The tests were performed using a universal testing machine (Zwick/Roell Z1.0, Zwick GmbH & Co. KG, Ulm, Germany) equipped with either 1 kN cell (tensile) or 0.5 kN cell (compression). Before the tensile tests, membranes were cut into rectangular samples (20 mm × 45 mm) and pressed into flat pieces (thickness of 1 mm). Then, the samples were mounted between two clamps (the gauge length was 15 mm for all samples) and subjected to deformation at a rate of 50 mm/min, while the pre-load was 1 N. The maximum stress and elongation at break were estimated using the TestXpert@II software. Young's modulus values were calculated from the stress–strain relationship. For the compressive test, membranes were cut into 2 cm × 2 cm rectangular pieces and placed between two metal plates. The direction of compression (at a rate of 50 mm/min) was perpendicular to the surface of the sample (the pre-load was 5 N). Values of the compressive modulus were calculated from the slope of linear stress–strain curves. Both the measurements were performed in 12 replicates.

2.4.5. Water Holding Capacity (WHC)

The WHC measurements were conducted according to [32]. Briefly, rectangular pieces (2 cm × 2 cm) of never-dried BNC/κ-Car membranes were quickly shaken twice and weighted to determine the wet mass. Then, they were dried in a vacuum gel dryer (Model 543, Bio-Rad, Hercules, CA, USA) at 80 °C for 4 h until the constant weight. Water holding capacity was calculated from the following equation:

$$WHC \left(g_{water}/g_{dry\ mass} \right) = \frac{W_W - W_d}{W_d} \tag{1}$$

where W_d is the weight of dry membrane and W_W is the weight of wet membrane. The experiment was carried out in triplicate for each BNC/κ-Car composite.

2.4.6. Swelling Properties and Water Retention Ratio (WRR)

The swelling ratio was determined by placing lyophilized, round-shaped BNC/κ-Car membranes with diameter of 38 mm, in distilled water. The samples were removed from water after certain period of time, initially after 10 min, and an excess water was gently drained with filter paper. Afterwards, samples were weighted. The content of water in swollen membranes was calculated using the following equation:

$$Swelling\ ratio\ \left(g_{water}/g_{dry\ mass}\right) = \frac{W_W - W_d}{W_d} \tag{2}$$

where W_d is the initial weight of dry sample and W_W is the weight of the wet membrane after incubation in distilled water. All the measurements were performed in triplicate.

To estimate the WRR values, the round-shaped, wet BNC/κ-Car membranes with a diameter of 38 mm, were weighted at different time intervals according to [33] until the complete water evaporation. Samples were stored at ambient temperature between measurements. Then, the percentage of water remained in BNC/κ-Car membranes was plotted against the time. Tests were done in triplicate for all the BNC/κ-Car composites.

2.5. ATDC5 Cell Viability Study

2.5.1. ATDC5 Cell Culture

The chondrogenic ATDC5 cell line originating from mouse teratocarcinoma AT805 was purchased from The Health Protection Agency (supplied by Sigma Aldrich, St. Louis, MO, USA). The cells were cultured in Dulbecco's Modified Eagle Medium: Nutrient mixture F12 (1:1; DMEM:F12) supplemented with 2 mM glutamine, 5% Fetal Bovine Serum (FBS), 100 U/mL penicillin, 100 mg/mL neomycin, and 2.5 μg/mL amphotericin B. All the culture medium components were obtained from the Life Technologies (Carlsbad, CA, USA). Cells were incubated at 37 °C in a humidified atmosphere supplemented with 5% CO_2.

2.5.2. Seeding of ATDC5 Cells on Scaffolds

Round-shaped BNC, κ-Car and BNC/κ-Car membranes were placed in 24–well polystyrene plates and soaked in complete the DMEM:F12 medium for 24 h. Then an excess of the culture medium was removed and ATDC5 cells were seeded into the prepared scaffolds at a density of 1.5×10^5 per well in the complete medium. Cells were incubated at 37 °C and 5% CO_2 for the next 21 days with medium exchange every 2–3 days. During ATDC5 cells culture, the morphology was observed and documented with a Leica M205 microscope (Leica Microsystems GmbH, Wetzlar, Germany) equipped with a Leica MC170 HD camera (Figure A2).

2.5.3. Cell Viability Assay

After 21 days of growth, the BNC, κ-Car and BNC/κ-Car scaffolds with ATDC5 cells were transferred into new 24-well plates (to reduce the false positive response from cells adhered to the plastic surface of wells). Subsequently, 500 μL of DMEM:F12 medium was added to each well and the number of viable cells was quantified by PrestoBlue viability assay. 40 μL of PrestoBlue cell viability reagent (Life Technologies, CA, USA), a resazurin-based solution, was added into each well and incubated further for 90 min at 37 °C and 5% CO_2. The number of viable cells was determined based on measurements of the fluorescent signal $F_{530/590}$ using a Synergy 2 Microplate Reader (Bio-Rad, CA, USA). Values of fluorescence magnitudes were used to calculate cell viability expressed as a percentage of the viability of the cells growing on the surface of BNC/κ-Car or κ-Car in comparison to pure BNC

$$viability\ [\%] = \frac{RFU_{sample} - RFU_{medium}}{RFU_{control} - RFU_{medium}} \cdot 100 \tag{3}$$

where RFU_{sample} is the fluorescence of cells growing on the BNC/κ-Car composites, RFU_{medium} is the fluorescence of medium without cells and $RFU_{control}$ is the fluorescence of cells, which grew on the BNC surface.

2.5.4. Gene Expression Analysis

After 21 days of ATDC5 cells growth, the BNC and BNC/κ-Car scaffolds were transferred to Falcon test tubes and washed twice with 2 mL of phosphate buffer saline. Subsequently, 1.5 mL aliquots of 0.25% trypsin/EDTA solution were added to detach ATDC5 cells. The suspensions of cells were collected and the density of cells was determined. Templates for one step real-time RT-PCR, without RNA extraction process, were prepared from 1.0×10^4 cells using a CellAmp Direct RNA Prep Kit (Takara Bio Inc., Kusatsu, Japan) according to the manufacturer's instructions. Primers (Table 1) were designed using the NCBI's Primer-BLAST software (National Center for Biotechnology Information) based on sequences from the GenBank database and purchased from Genomed, Poland.

Table 1. Primers designed to amplify selected genes for real time RT-PCR analysis.

Gene	Forward Primer	Reverse Primer	Acc. No.
Col1α1	5′-ATGCCGCGACCTCAAGATG-3′	5′-TGAGGCACAGACGGCTGAGTA-3′	NM007742
Col2α1	5′-AGGGCAACAGCAGGTTCACATAC-3′	5′-TGTCCACACCAAATTCCTGTTCA-3′	NM031163
Runx2	5′-CACTGGCGGTGCAACAAGA-3′	5′-TTTCATAACAGCGGAGGCATTTC-3′	NM009820
Sox9	5′-TCCCCGCAACAGATCTCCTA-3	5′-AGGTGGAGTAGAGCCCTGAG-3′	NM011448
Gapdh	5′-AAGGCTGGGGCTCATTTGCAGG-3′	5′-GCCAGGGGTGCTAAGCAGTTGG-3′	NM002046

Quantitative reverse transcription-polymerase chain reaction (qRT-PCR) was performed using a One Step PrimeScript™ RT-PCR Kit (Takara Bio Inc., Kusatsu, Japan) and a CFX96™ detection system (Bio-Rad, Hercules, CA, USA). The process started with reverse transcription (5 min; 42 °C) and cDNA melting (10 s; 95 °C). 40 cycles of real time-PCR consisted of denaturation (5 s; 95 °C), annealing (30 s; 60 °C), and elongation (30 s; 72 °C). Nonspecific products and primer dimers were excluded by melting curve analysis performed by maintaining the temperature at 50 °C for 2 s, followed by a gradual increase in temperature to 95 °C. The final products were separated electrophoretically on a 2.7% agarose gel in TAE buffer (TRIS/acetate/EDTA) containing a nucleic acid stain (Midori Green Advance DNA stain, NIPPON Genetics, Tokyo, Japan). Constitutively expressed GAPDH gene was selected as an endogenous control. Expression of examined genes were normalized to GAPDH expression and control samples genes expression. The target gene expression levels were calculated using the Livak and Schmittgen equations [34]:

$$\Delta C_{t,sample} = C_{t,target \ gene \ for \ sample} - C_{t,GAPDG \ for \ sample} \tag{4}$$

$$\Delta C_{t, \ control} = C_{t,target \ gene \ for \ control} - C_{t,GAPDG \ for \ control} \tag{5}$$

$$\Delta\Delta C_t = \Delta C_{t,sample} - \Delta C_{t, \ control} \tag{6}$$

$$Relative \ gene \ expression = 2^{-\Delta\Delta C_t} \tag{7}$$

2.6. Statistical Analysis

Statistical significance of data was evaluated by analysis of variance (ANOVA; $p < 0.05$) using the MiniTab18 software. For significant effects the Tukey method of multiple comparisons was performed.

3. Results and Discussion

3.1. Biosynthesis of BNC and BNC/κ-Car Composites

BNC/κ-Car composites were biosynthesized in situ using two methods, which exploited the viscoelastic behavior of κ-Car chains in *aqueous* solutions. In the first method, κ-Car (0.2, 0.5 and 0.8%)

was added to the SH culture medium and sterilized. Above the temperature of 70 °C, κ-Car forms a colloidal solution and upon cooling, the double helices of biopolymer form a three-dimensional network. Afterwards, the growing BNC penetrated κ-Car matrix and the compact structure of the composite was formed. The viscosity of culture medium grew with the increasing concentration of κ-Car. This in turn decreased the oxygen transfer rate and reduced BNC formation. The similar observation was reported in case of aloe vera juice addition to a culture medium [35].

In the second method, sterile κ-Car was added to the cooled SH culture medium previously supplemented with 2.0 g/L κ-Car. Under such conditions, the supplementary κ-Car did not form the gel spontaneously. Instead, it formed large agglomerates whose appearance was ascribed to formation of water layer around each κ-Car coil. Strong stirring allowed to obtain stable homogenous medium containing 2, 4 and 6 of κ-Car on the basis of the matrix created by 0.2% κ-Car. During cultivation, cellulose fibers surrounded the κ-Car agglomerates and formed the loose 3D network. The increase in κ-Car concentration resulted in a decrease in the BNC composite mass. In the case of BNC/κ-Car$_{6.0}$ very thin and soft pellicle was obtained and therefore it was excluded from further characterization.

Both the in situ methods allowed to obtain new and unique structures of membranes. The presence of κ-Car in the BNC-based membranes strongly affected their properties, such as fibers morphology, chemical composition, crystallinity, tensile and compression strength, water holding capacity, water retention ratio, and swelling properties.

3.2. Characterization of BNC/κ-Car Composites

3.2.1. Morphology and Fibers' Architecture of BNC/κ-Car Composites

Bionanocellulose sub-elementary fibrils, which are 3–6 nm in diameter, and are extruded by bacterial cells during cultivation, immediately form microfibrils and crystallize, yielding type I cellulose [36]. The network of fibers is compact and diameters of single fibers are around 40–60 nm (Figure 1a). Medium viscosity has a great impact on the bacterial cellulose structure. According to [37] BNC synthesized in viscous culture media consist of bundles, which either represent type II cellulose or contain a mixture of type I and type II cellulose.

The structure of composites produced by the first method, was slightly different from the structure of BNC derived from the unmodified SH medium (Figure 1b–d). The spaces between cellulose fibers, visible in the Figure 1, were enlarged when the concentration of κ-Car in the culture medium was increased. Only in case of the BNC$_{0.2}$ composite, which was obtained at a relatively low κ-Car concentration, the empty spaces between BNC fibers were not visible. We assume that the medium viscosity as well as adhesion of κ-Car to cellulose ribbons significantly influenced the diameter of fibers in case of BNC κ-Car$_{0.5}$ and BNC κ-Car$_{0.8}$. The average diameters of strands were 83 nm and 119 nm, respectively (Figure 2c,d). The latter value was 2.4-fold greater compared to the unmodified BNC fibers.

The second method resulted in formation of highly porous structures of both BNC/κ-Car$_{2.0}$ and BNC/κ-Car$_{4.0}$ composites (Figure 1e,f). Winding of cellulose ribbons around κ-Car agglomerates gave rise to the very loose 3D network. Furthermore, most of κ-Car was incorporated into the surface layers of membranes that was visible in SEM images. Therefore, despite the increased porosity, the latter composites were relatively rigid, as the compression modulus indicated (Section 3.2.5). The diameters of fibers were reduced to 48 and 35 nm for BNC/κ-Car$_{2.0}$ and BNC/κ-Car$_{4.0}$, respectively (Figure 2e,f).
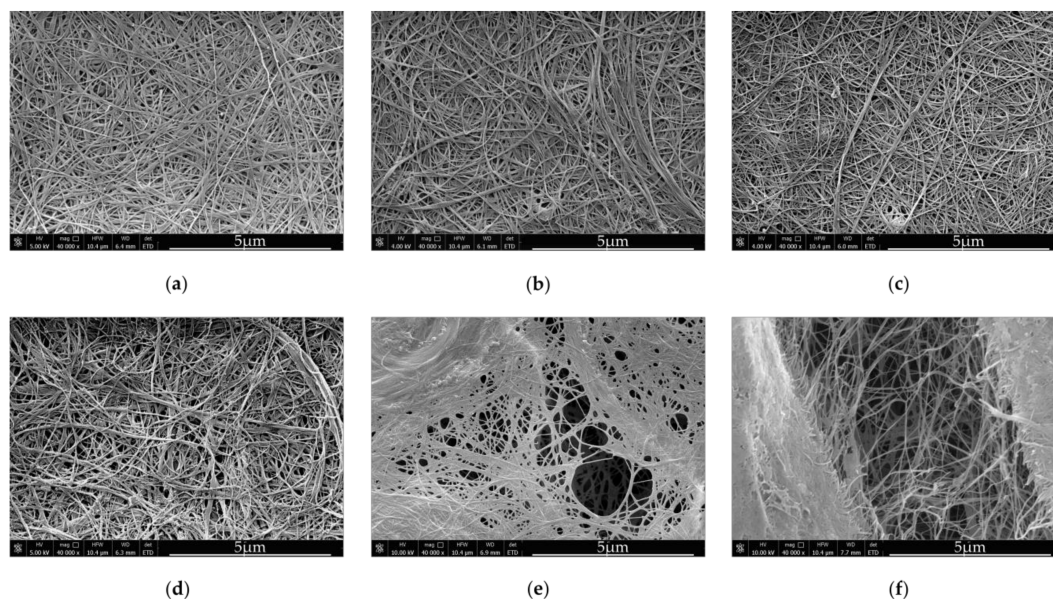
Figure 1. Scanning electron microscope (SEM) images of cellulose nanofibers in (**a**) BNC, (**b**) BNC/κ-Car$_{0.2}$, (**c**) BNC/κ-Car$_{0.5}$, (**d**) BNC/κ-Car$_{0.8}$, (**e**) BNC/κ-Car$_{2.0}$, and (**f**) BNC/κ-Car$_{4.0}$. The images were recorded at the magnification of 40,000× (bar—5 μm).

Figure 2. Fibers width (nm) distribution in (**a**) BNC, (**b**) BNC/κ-Car$_{0.2}$, (**c**) BNC/κ-Car$_{0.5}$, (**d**) BNC/κ-Car$_{0.8}$, (**e**) BNC/κ-Car$_{2.0}$ and (**f**) BNC/κ-Car$_{4.0}$.

3.2.2. FTIR-ATR Analysis

The FTIR spectra of BNC, κ-Car and BNC/κ-Car composites are presented in Figure 3. Samples were scanned over the range of 4000–650 cm^{-1} to observe the effect of κ-Car presence in BNC membranes, caused by the in situ modification.

In the case of pure BNC, two main peaks can be observed. A sharp characteristic peak of O-H stretching appears at 3347 cm^{-1} and another important peak of 1645 cm^{-1} is assigned to the glucose carbonyl stretching [38,39]. A series of bands from 1200 to 1000 cm^{-1} are related to the stretching

of C-O-C of sugar rings and C-O stretching vibrations of the primary (C_6) and secondary hydroxyl (C_2, C_3) groups. CH_2 deformation can be detected at 1428 cm^{-1}. The absorption band at 2896 cm^{-1} corresponds to CH-stretching and CH_2 asymmetric stretching [40]. The peak at 1316 cm^{-1} results from CH_2 wagging symmetric bending [41].

The FTIR spectrum of κ-Car demonstrates peaks, which are characteristic of this polymer. The absorption bands at 1234, 929, and 844 cm^{-1} are assigned to S=O of sulfate esters, C-O of anhydrogalactose and sulfation of C_4 on galactose [42], respectively. Sulfonic acid groups can be indicated based on the peak at 1368 cm^{-1} [43]. The spectra of BNC/κ-Car composites provided evidence that the main component of these composites is cellulose. However, these spectra contain additional small peaks in the range of 1260–1240, 940–920 and 810–845 cm^{-1}, which are typical of κ-Car. The band's shape at 1030 cm^{-1} suggests mixing of two peaks from both the polysaccharides. Shifting of absorption band of $CO-SO_3$ of the β-1,3-linked residue from 845 to 810 cm^{-1} can be observed in the case of all the composites. The shift may be ascribed to the interactions of cellulose chains with κ-Car coils. The region of 3600–3000 cm^{-1}, which corresponds to –OH stretching is broader in the case of BNC/κ-Car, especially in case of BNC/κ-Car$_{2.0}$ and BNC/κ-Car$_{4.0}$, in comparison to the native BNC. This may suggest the interleaving of cellulose fibers and carrageenan matrix and occurrence of physical interactions between these biopolymers via additional hydrogen bonds. The latter effect was observed also for BNC composites with other compounds such as sodium alginate [44], agarose [45], chitosan [46], and collagen [47].
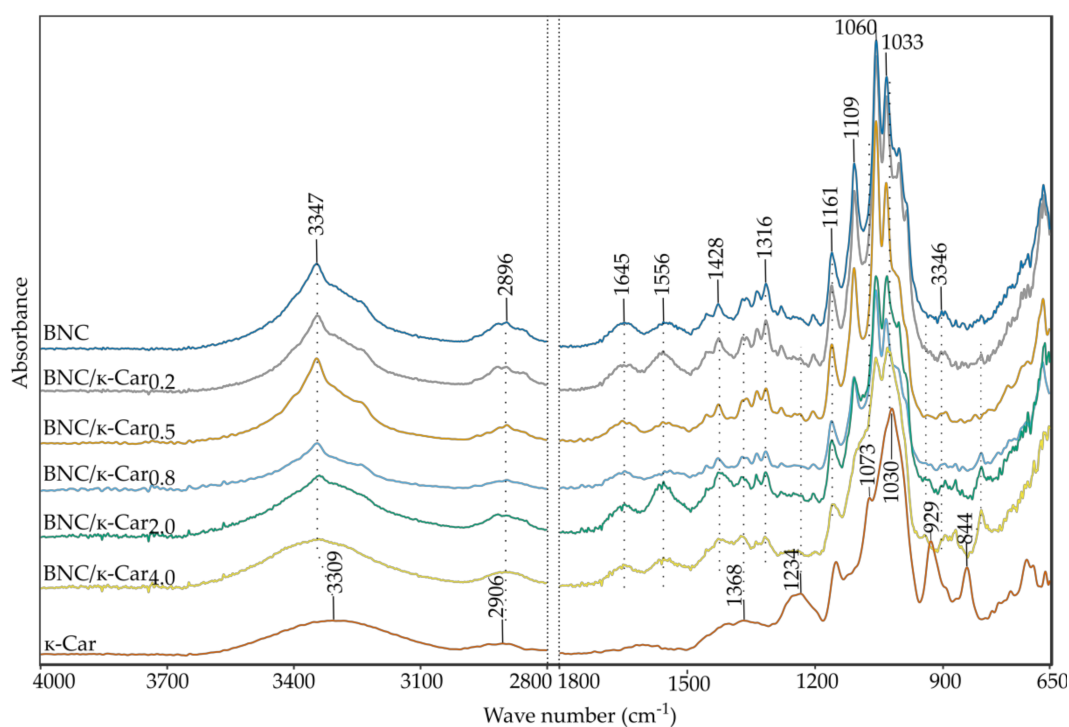

Figure 3. The Fourier-transform infrared spectroscopy (FTIR) spectra of BNC, κ-Car and BNC/κ-Car composites at wave numbers ranging from 4000 to 650 cm^{-1}.

3.2.3. X-ray Diffraction (XRD) Analysis

The XRD method was used to determine the crystallinity index (CI) of the BNC/κ-Car composites (Table 2). The diffraction patterns (Figure 4) contain three main peaks that are present at ~14.66°, ~17.26° and ~22.90° for the (101), (10–1) and (200) planes, respectively, and they may be identified as the reflection planes of cellulose I [30]. The peaks in the diffraction curve of all the samples were relatively broad, because BNC contains amorphous regions apart from the crystalline areas. With the

increase of κ-Car concentration, the CI of BNC/κ-Car decreased, from 87.6% for pure BNC to 77.4% for BNC/κ-Car$_{4.0}$. This may suggest the occurrence of interactions between cellulose ribbons and helices or coils of κ-Car during crystallization process. These results are consistent with the FTIR data.

Table 2. Crystallinity index (CI) of BNC/κ-Car composites.

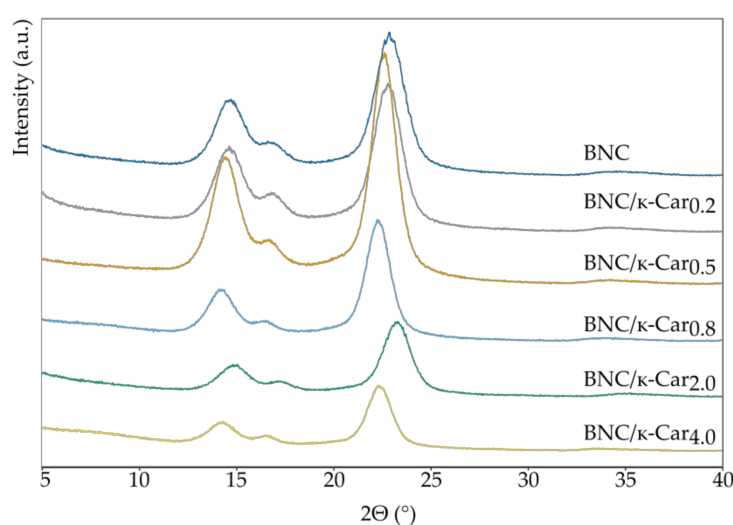| Sample	CI (%)
BNC	87.6
BNC/κ-Car$_{0.2}$	85.7
BNC/κ-Car$_{0.5}$	85.3
BNC/κ-Car$_{0.8}$	85.0
BNC/κ-Car$_{2.0}$	79.8
BNC/κ-Car$_{4.0}$	77.4

Figure 4. XRD diffraction patterns of BNC/κ-Car composites.

3.2.4. Water Holding Capacity, Water Retention Rate, and Swelling Properties

Water holding capacity, water retention rate and swelling properties are very important parameters with regard to medical applications of biomaterials. They decide of water diffusion in membrane and thus the ability of transporting the nutrients and active compounds throughout the biomaterial. The high water retention capacity enables to maintain the moist environment that is crucial for the proper cell growth and favorable interactions with the environment in tissue engineering applications.

The results of WHC measurements for the pure BNC and composites with κ-Car are shown in Figure 5. The highest water content was observed for BNC and BNC/κ-Car$_{0.2}$ (it reached 137 and 133 g water/g of their dry mass, respectively). However, we observed a decline in WHC for higher concentrations of κ-Car (0.5 and 0.8%). WHC was reduced to 109 $g_{water}/g_{dry\ mass}$ in case of BNC/κ-Car$_{0.8}$. WHC level is a consequence of structural arrangements of fibrils in BNC network and it is affected by the size of pores, crystallinity index, density, and width of fibers. The addition of gelling agents such as carrageenan or agar to the culture medium resulted in the changed cellulose network consisting of ribbon-like wide fibers [48]. The contact surface was decreased and less water molecules could be hold within the BNC structure [49]. On the other hand, the presumable reason of the reduced WHC in the case of BNC/κ-Car$_{2.0}$ and BNC/κ-Car$_{4.0}$ (117 and 123 $g_{water}/g_{dry\ mass}$, respectively) was the presence of κ-Car aggregates, especially in surface layers, which filled the empty spaces between fibers.
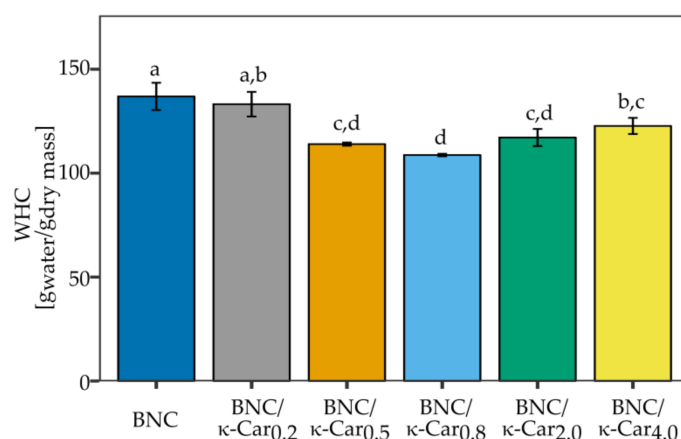
Figure 5. Water holding capacity of BNC and BNC/κ-Car composites (The data are presented as the means ± SD from at least three independent experiments; the means that are marked with different letters are significantly different).

The swelling ability of hydrogels is essential in tissue engineering and drug delivery applications. During the process of swelling, the structure of the porous materials changes due to the growing distance between the fibers. The absorbed water molecules are directed to free spaces, fill them, and form hydrogen bonds with chains of polymers. Both BNC and κ-Car are excellent water absorbents, and therefore they have found numerous medical applications. However, their swelling profiles are different. Pure κ-Car, which can absorb 11.28 g water per 1 g of its dry mass, swells rapidly and the gel reaches the equilibrium state in 60 min (Figure A1). BNC swells more slowly and binds 87.75 $g_{water}/g_{dry\ mass}$, what is 7.8 times more compared to κ-Car. Water completely fills pores in BNC membranes within 3 h (Figure 6). In the case of BNC/κ-Car$_{0.2}$, BNC/κ-Car$_{0.5}$, and BNC/κ-Car$_{0.8}$, the amount of absorbed water decreased when the concentration of κ-Car in the culture medium increased (79.13, 64.26, and 53.27 $g_{water}/g_{dry\ mass}$, respectively). These results were consistent with the data obtained for BNC and pure κ-Car. The swelling ratio of BNC/κ-Car composites reflected both the water binding capacity of each of the two biopolymers and their percentages in the composites.

The swelling profiles for BNC/κ-Car$_{2.0}$ and BNC/κ-Car$_{4.0}$ were different compared to the other composites. The plateau was achieved after 36 and 48 h, respectively. After 3 h, when BNC was completely hydrated, the degrees of swelling of BNC/κ-Car$_{2.0}$ and BNC/κ-Car$_{4.0}$ were only 55 and 53%, respectively. This difference may be ascribed to the high concentration of κ-Car in surface layers since the latter polymer swells quickly but binds less water. The occurrence of negative charges on its coils causes that water molecules to bind strongly and their diffusion to the interior of the membrane takes more time. BNC/κ-Car$_{2.0}$ and BNC/κ-Car$_{4.0}$ absorbed 70.52 and 95.65 $g_{water}/g_{dry\ mass}$, respectively. The difference in the swelling ratio is a consequence of different porosity and contact surface area, which are greater in the case of BNC/κ-Car$_{4.0}$ and therefore, the latter composite bound more water.

The water retention rate of BNC and its composites is a vital parameter in case of medical applications [50]. Like WHC, WRR is affected by the thickness and structure of fibers as well as the presence of additives inside the membrane [33]. Interestingly, the WRR profiles of the BNC/κ-Car composites obtained in this study were different from the WHC profiles. In case of BNC/κ-Car prepared by the first method, the rate of water evaporation decreased with the increase in κ-Car concentration, with an exception of BNC/κ-Car$_{0.8}$ (Figure 7). The similar observations were reported by [51] who studied the effect of an increasing concentration of a single sugar on the α-linked glucuronic acid-based oligosaccharide. The positive impact of carrageenan on WRR of carrageenan/hydroxymethyl cellulose composites was also reported [52]. In this study, the differences between the composites were visible after 6 h of drying process. Presumably, the molecules of water, which were physically attached to the surface of membranes, were evaporated within this

time. Noteworthy, these molecules accounted for less than 20% of bound water. The diffusion of the remaining water molecules, which were entrapped between the fibers, took either 36 h (BNC) or 48 h (BNC/κ-Car$_{0.2}$ and BNC/κ-Car$_{0.5}$). The composite BNC/κ-Car$_{0.8}$ was characterized by the significantly lower value of WRR that may be ascribed to the high thickness of fibers and enhanced porosity, which were visible in the SEM images. Presumably, these parameters had the greater impact on WRR than the presence of κ-Car. Because of the lower surface area and expanded pores, water molecules that are bound either to the surface or inside the membrane may be removed much easier. WRR values of BNC/κ-Car$_{2.0}$ and BNC/κ-Car$_{4.0}$ were similar and water evaporation took up to 48 h. The effect of κ-Car incorporation into the surface layers of membranes was noticeable. The diffusion of water was hindered like in case of the swelling behavior of modified BNC and within 24 h, BNC/κ-Car$_{2.0}$, BNC/κ-Car$_{4.0}$ and BNC lost 55, 60 and 68% of bound water, respectively.
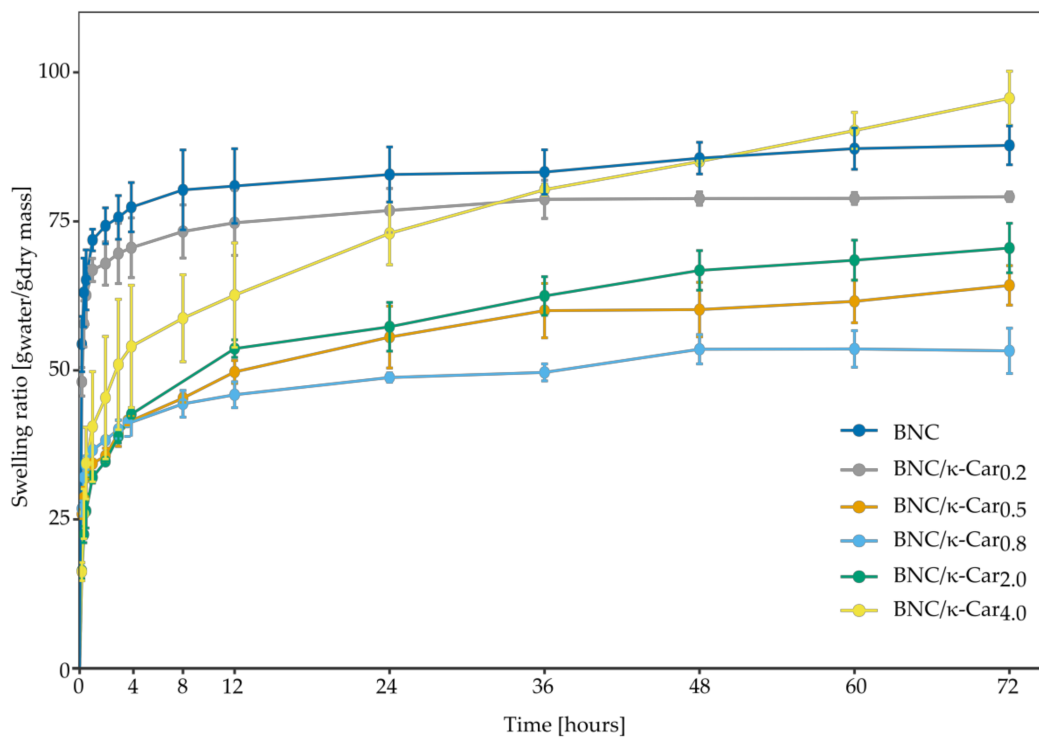

Figure 6. Swelling ratio of BNC and BNC/κ-Car composites. (The data are presented as the means $\pm$ SD from at least three independent experiments).
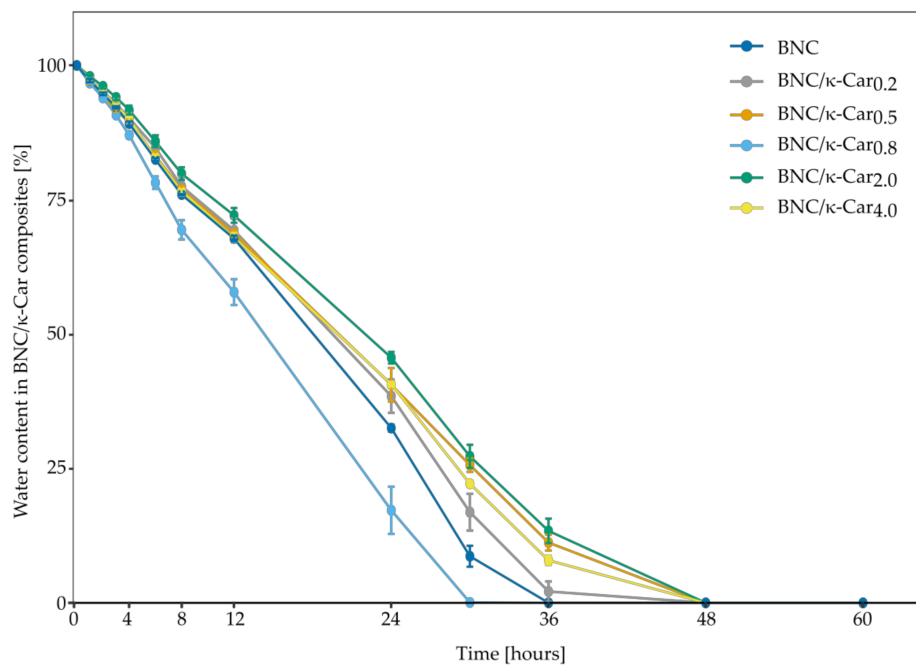
Figure 7. Water retention ratio of BNC and BNC/κ-Car composites. (The data are presented as the means ± SD from at least three independent experiments).

3.2.5. Mechanical Strength

Tissue engineering applications commonly encompass the use of scaffolds to provide a suitable microenvironment for the incorporation of cells to regenerate damaged tissues or organs. Scaffolds should exhibit high mechanical strength to maintain integrity until new tissue regeneration. It is especially important in case of cartilage tissue replacements. As the load bearing material, cartilage functions in a challenging mechanical environment. Bacterial nanocellulose is known as a mechanically stable biomaterial with hydrogel-like characteristic [53]. Interestingly, incorporation of κ-Car into BNC additionally improved the tensile strength of BNC/κ-Car composites at κ-Car concentrations up to 2% (Table 3). Also, the elongation at break was affected by the incorporation of κ-Car. In the case of the second method of BNC/κ-Car production, the fracture strain was increased to 163 and 180% compared to the native BNC for BNC/κ-Car$_{2.0}$ and BNC/κ-Car$_{4.0}$, respectively. The Young's modulus of the native articular cartilage is about 10 MPa [54,55]. All the composites obtained in this study, with an exception of BNC/κ-Car$_{4.0}$, were characterized by the higher tensile modulus values ranging from 12.32 to 16.35 MPa, in contrast to pure BNC, whose Young's modulus was below 9 MPa.

Table 3. Mechanical strength of BNC/κ-Car composites (The data are presented as the means ± SD from at least twelve independent experiments; the means that are marked with different letters are significantly different).

Sample	Tensile Strength			Compression
	Stress (MPa)	Elongation (%)	Young's Modulus (MPa)	Young's Modulus (MPa)
BNC	2.01 [c] ± 0.24	28.16 [c] ± 1.80	8.96 [c] ± 1.28	7.44 [c] ± 0.81
BNC/κ-Car$_{0.2}$	2.22 [c] ± 0.31	21.89 [d] ± 1.07	12.82 [b] ± 1.57	7.48 [c] ± 0.70
BNC/κ-Car$_{0.5}$	2.73 [b] ± 0.42	23.22 [d] ± 1.14	16.35 [a] ± 2.34	5.63 [d] ± 0.40
BNC/κ-Car$_{0.8}$	2.95 [b] ± 0.26	31.71 [c] ± 2.97	12.32 [b] ± 1.11	4.90 [d] ± 0.38
BNC/κ-Car$_{2.0}$	4.86 [a] ± 0.58	45.79 [b] ± 5.79	12.64 [b] ± 1.27	14.31 [b] ± 1.55
BNC/κ-Car$_{4.0}$	3.10 [b] ± 0.46	50.50 [a] ± 4.53	7.46 [c] ± 0.90	16.21 [a] ± 1.60

As components of cartilage tissue, the chondrocytes are adapted to function under elevated pressure, and mechanical compression is thought to stimulate the proliferation and differentiation of these cells [56,57]. Therefore, the compression modulus is the key parameter, which determines the utility of scaffolds in tissue engineering. The study of Toyoda et al. showed that exposition of chondrocytes seeded in a three-dimensional agarose scaffold on the static or pulsing hydrostatic pressure of 5 MPa for 4 h resulted in the increasing of GAG synthesis and a four-fold higher level of aggrecan mRNA [56]. In the case of BNC and BNC-based composites, the compression properties depend on the arrangement and thickness of fibers as well as the porosity and crystallinity of membranes. The compression of samples between plates causes the removal of water. In case of the composites produced by the first method, the results of measurements of compression properties were consistent with the results of water holding capacity measurements and correlated with their porosity. Upon compression, water entrapped inside the membrane causes the resistance and immediately flows out.

Interestingly, the composites BNC/κ-Car$_{2.0}$ and BNC/κ-Car$_{4.0}$ behaved in an unusual manner. Despite the large free spaces between thin fibers, the lower WHC and decline in crystallinity, in comparison to the native BNC, were observed. The compression modulus was 1.9 and 2.2 times higher for BNC/κ-Car$_{2.0}$ and BNC/κ-Car$_{4.0}$, respectively, than for BNC. Presumably, the incorporation of κ-Car into the surface layers of membranes caused that the removal of water from the composites was impeded. BNC modified in that way may have a great potential in TE of cartilage connected with mechanical stimulation of chondrocytes, leading to a higher efficacy of their cultivation.

3.3. The Viability of ATDC5 Cells

To evaluate the usefulness of BNC/κ-Car composites as a scaffold material for cartilage repair, cell viability was assessed with Presto Blue® test. The effect of the scaffold on the viability of ATDC5 cells is presented in Figure 8.
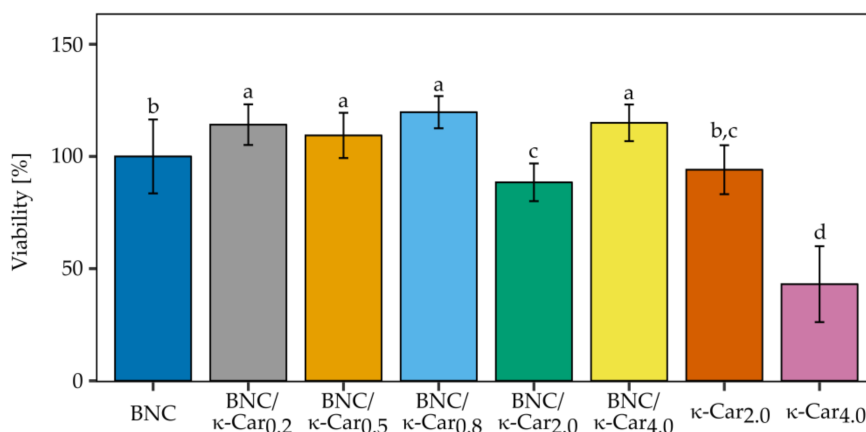

Figure 8. The viability of ATDC5 cells after 21 days of growing on the surface of BNC and BNC/κ-Car composites. (The data are presented as the means $\pm$ SD from at least three independent experiments; the means that are marked with different letters are significantly different).

As the biocompatibility of pure BNC produced by *K. xylinus* E25 is well known [58] the significant differences in the viability of cells cultivated on the BNC control and nearly all BNC/κ-Car composites were promising. After 21 days of growth on various BNC/κ-Car composites ATDC5 cells exhibited the increased cell viability in comparison to the BNC control sample. The only exception was BNC/κ-Car$_{2.0}$, for which the ATDC5 cells viability was reduced to 88.5%. The growth of the cells on pure 2 and 4% κ-Car gels was also monitored (at the lower concentrations, κ-Car does not form stable gels). The observed high toxicity of 4% κ-Car was consistent with data obtained by Sathuyan et al. [59], who

reported the correlation between κ-Car concentration and cell viability, and showed that the growing polysaccharide concentration caused the decrease in cell viability, which depended also on the time of growth.

3.4. Relative Gene Expression

Apart from determination of the ATDC5 cells viability, also the relative expression of the selected genes, which are crucial for the process of chondrogenesis, was under scrutiny (Figure 9). The long expansion time and multiple passaging often lead to "dedifferentiation" of chondrocytes, which is defined as the gradual loss of differentiation molecular markers. Chondrocytes cultivated in vitro on the plastic surfaces dedifferentiate particularly quickly to less specific cells with enhanced ability to proliferate [60]. As dedifferentiation progresses, the expression of genes encoding the extracellular matrix components, such as collagen type II (*Col2a1*) or SRY (sex determining region Y)-box 9 (*Sox9*), transcription factor is changed, whilst at the same time the cells acquire an increased fibroblastic phenotype, characterized by the expression of the genes encoding collagen type I (Col1a) or runt related transcription factor 2 (*Runx2*) [61]. Specifically, *Sox9* transcription factor enhances expression of *Col2a1* while overexpression of *Runx2* is connected with the appearance of hypertrophic chondrocytes and leads to the appearance of osteoblasts followed by cell mineralization [61,62].

It was shown that some biophysical stimuli, like three-dimensional space for growth, are sufficient for cells to differentiate to chondrocytes [63]. The surfaces of BNC scaffolds were uneven with a porous structure, which allowed the cells to penetrate into the biopolymer structure. Therefore, pure BNC scaffolds slightly enhanced the differentiation process [14,58]. What is more, some findings proved that the negatively charged surfaces of scaffolds could promote cell dedifferentiation [64].

The *Col1α1* expression was found to be nearly the same in case of all BNC/κ-Car composites as compared to the ATDC5 cells growing on either plastic surface (data not shown) or pure BNC. In case of the majority of BNC/κ-Car composites the expression level of *Col2α1* was slightly higher than in the control sample. The only exception, for which the level of expressed *Col2α1* was statistically increased was the BNC/κ-Car$_{0.8}$ composite. *Sox9* expression was significantly enhanced in case of all the composites with higher κ-Car concentration, namely BNC/κ-Car$_{0.5}$, BNC/κ-Car$_{0.8}$, and BNC/κ-Car$_{2.0}$. Finally, low expression level of *Runx2* shows that none of the composites tested induced the chondrocyte hypertrophy. Thus, the results of this study showed that BNC/κ-Car composites supported the dedifferentiation of ATDC5 cells to more chondrogenic phenotype, as demonstrated by the increase in the expression of chondrogenic marker genes *Col2α1*, *Sox9* and the decrease of *Col1α1* and *Runx2* expression.
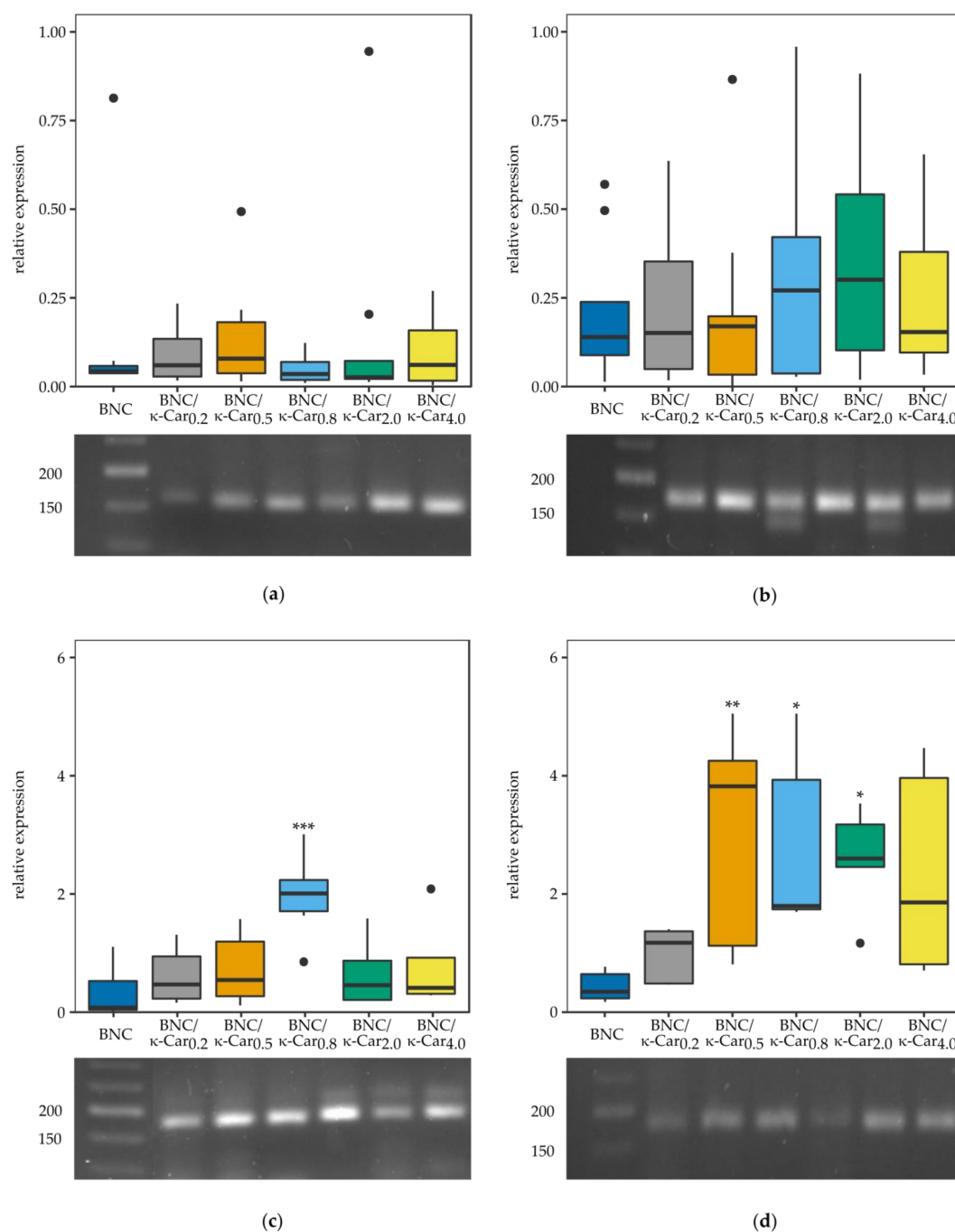
Figure 9. The relative expression of selected genes involved in differentiation of the ATDC5 cell line. Examined genes: (**a**) *Col1α1*, (**b**) *Runx2*, (**c**) *Col2αl* and (**d**) *Sox9*. Multiple comparison was assessed by One-way ANOVA. Statistical significance shown as:* $p < 0.05$, ** $p < 0.01$, *** $p < 0.001$ in comparison to ATDC5 cells growing on the surface of the unmodified BNC scaffold.

4. Conclusions

In this work, two variants of the innovative in situ method of novel bacterial cellulose/κ-carrageenan composites production, based on the stationary culture of GRAS bacteria *K. xylinus* E25, were established. It was shown that the method enables the production of BNC/κ-Car composites, which outperform the two polymers when used separately as potential scaffolds for tissue engineering, regarding the morphology of fibers, chemical composition, crystallinity, tensile

and compression strength, water holding capacity, water retention ratio and swelling properties. Also, the cultures of murine chondrogenic ATDC5 cells provided evidence of the utility of the BNC/κ-Car composites as scaffolds for TE. The positive effect of the composites on the cells viability and chondrogenic differentiation was measured as the expression patterns of *Col1α1*, *Col2α1*, *Runx2*, and *Sox9*. All the composites obtained in this study supported the differentiation of ATDC5 cells to more chondrogenic phenotype and none of them caused the chondrocyte hypertrophy.

Author Contributions: Conceptualization, Methodology and Writing-Original Draft Preparation, I.C., M.S., E.G.-D.; Formal Analysis and Investigation, I.C., M.S., W.M.; Writing-Review & Editing, H.K.; Visualization, M.R.; Supervision and Critical review, S.B.

Conflicts of Interest: The authors declare no conflict of interest.

Appendix A

Appendix A.1 Swelling Properties of κ-Car

κ-Car$_{0.2}$ gels were used in the swelling study. 2 g/L of κ-Car was dissolved in 0.1 M CaCl$_2$ during sterilization (121 °C for 20 min) and then immediately transferred under sterile conditions into a 6-well plate (well diameter of 38 mm, 10 mL per well). After gel formation, the samples were freeze-dried, weighted, and then placed in distilled water. κ-Car gels were removed from water every 10 min, gently drained with filter paper and weighted. The content of water in the swollen samples was calculated using Equation (2). All the measurements were performed in triplicate.
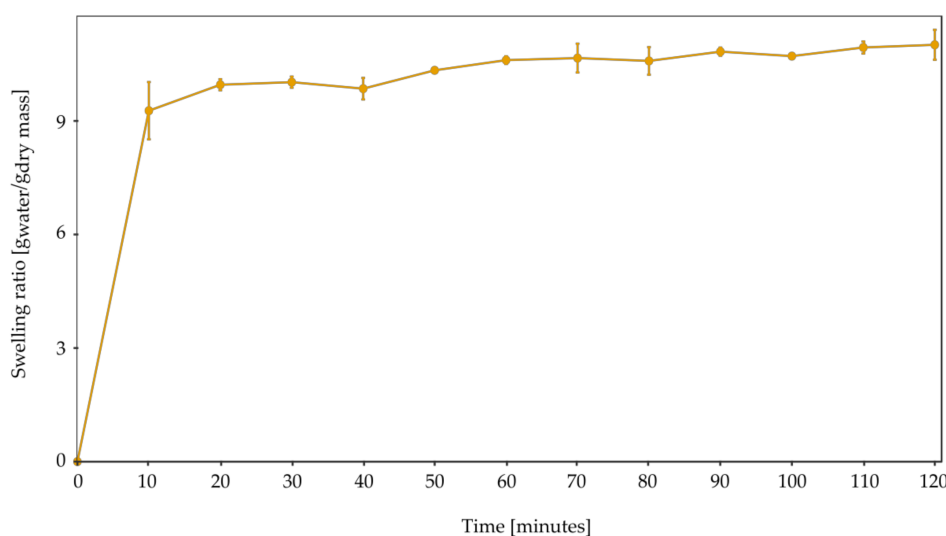

Figure A1. Swelling ratio of κ-Car$_{0.2}$ (The data are presented as the means ± SD from at least three independent experiments).

κ-Car gels swelled in 10 min and reached an equilibrium state after 60 min. After that the mass of swollen samples did not change significantly. The water absorption capacity of κ-Car was 11.28 g water per 1 g dry weight.

Appendix A.2 The Growth Morphology of ATDC5 Cells

The results of this study showed that the BNC/κ-Car composites supported the dedifferentiation of ATDC5 cells to more chondrogenic phenotype, as demonstrated by the increase in the expression of chondrogenic marker genes *Col2α1*, *Sox9* and the low level of *Col1α1* and *Runx2* expression. What

is more, their morphology was changed. Figure A2 presents ATDC5 cells growing on the different surfaces. In contrast to the adherent growth on the plastic surface (a) the cells on scaffolds (b–g) formed clusters characteristic of the matured chondrocytes.
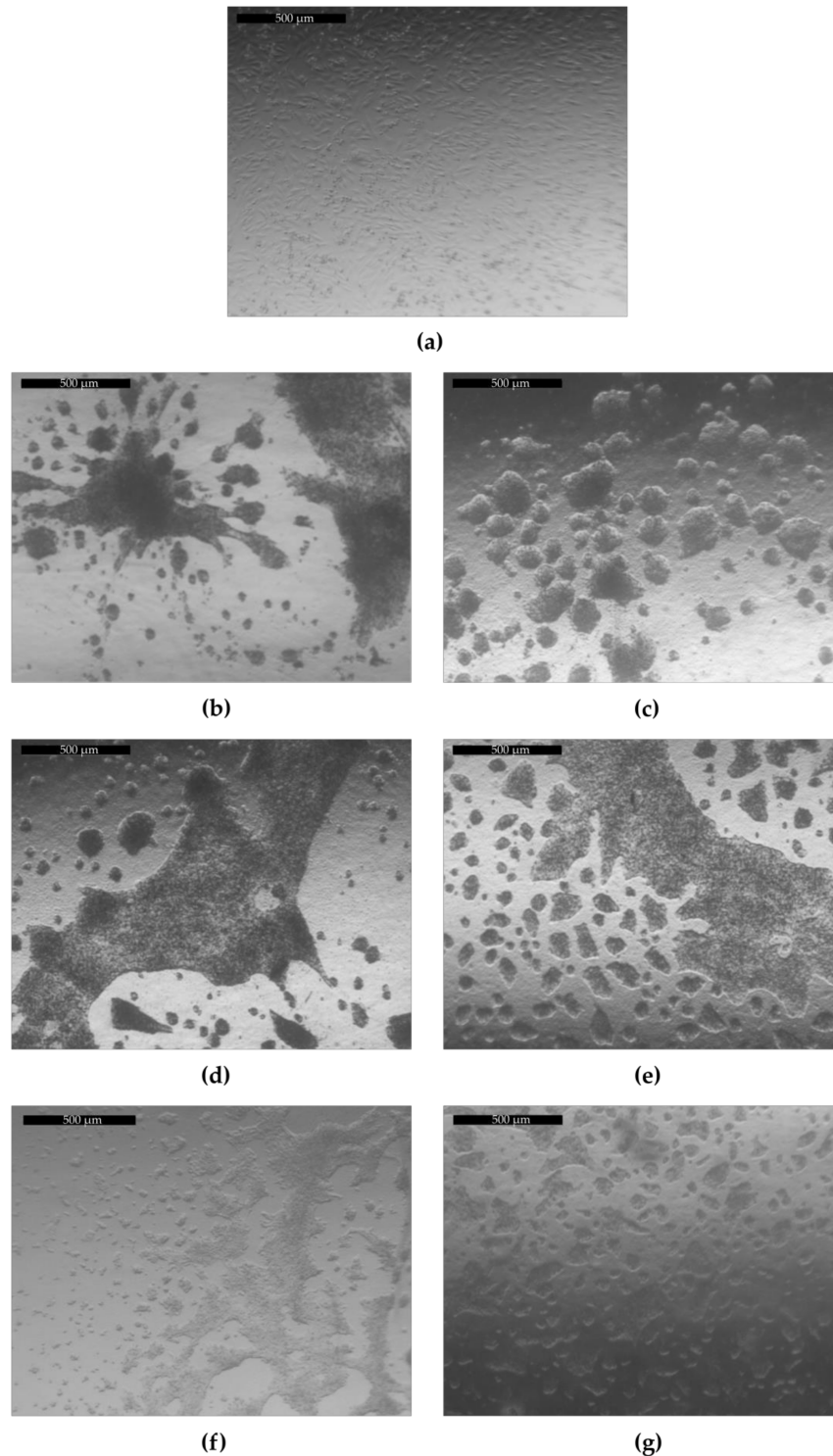

Figure A2. The ATDC5 cell growth morphology after 20 days of incubation on the surface of different scaffolds: (**a**) control growth on plastic, (**b**) growth on pure BNC scaffold, (**c**–**g**) growth on the surface on BNC/κ-Car composites: (**c**) BNC/κ-Car$_{0.2}$, (**d**) BNC/κ-Car$_{0.5}$, (**e**) BNC/κ-Car$_{0.8}$, (**f**) BNC/κ-Car$_{2.0}$, (**g**) BNC/κ-Car$_{4.0}$.

References

1. Gao, Y.; Liu, S.; Huang, J.; Guo, W.; Chen, J.; Zhang, L.; Zhao, B.; Peng, J.; Wang, Y.; Xu, W.; et al. The ECM-Cell interaction of cartilage extracellular matrix on chondrocytes. *BioMed Res. Int.* **2014**, e648459. [CrossRef] [PubMed]

2. Kessler, M.W.; Grande, D.A. Tissue engineering and cartilage. *Organogenesis* **2008**, *4*, 28–32. [CrossRef] [PubMed]

3. Vinatier, C.; Guicheux, J. Cartilage tissue engineering: From biomaterials and stem cells to osteoarthritis treatments. *Ann. Phys. Rehabil. Med.* **2016**, *59*, 139–144. [CrossRef] [PubMed]

4. Jozala, A.F.; de Lencastre-Novaes, L.C.; Lopes, A.M.; Santos-Ebinuma, V.C.; Mazzola, P.G.; Pessoa, A., Jr.; Grotto, D.; Gerenutti, M.; Chaud, M.V. Bacterial nanocellulose production and application: A 10-year overview. *Appl. Microbiol. Biotechnol.* **2016**, *100*, 2063–2072. [CrossRef] [PubMed]

5. Helenius, G.; Bäckdahl, H.; Bodin, A.; Nannmark, U.; Gatenholm, P.; Risberg, B. *In vivo* biocompatibility of bacterial cellulose. *J. Biomed. Mater. Res. Part A* **2005**, *76A*, 431–438. [CrossRef] [PubMed]

6. Lin, S.B.; Hsu, C.P.; Chen, L.C.; Chen, H.H. Adding enzymatically modified gelatin to enhance the rehydration abilities and mechanical properties of bacterial cellulose. *Food Hydrocolloids* **2009**, *23*, 2195–2203. [CrossRef]

7. Fontana, J.D.; de Souza, A.M.; Fontana, C.K.; Torriani, I.L.; Moreschi, J.C.; Gallotti, B.J.; de Souza, S.J.; Narcisio, G.P.; Bichara, J.A.; Farah, L.F. *Acetobacter* cellulose pellicle as a temporary skin substitute. *Appl. Biochem. Biotechnol.* **1990**, *24–25*, 253–264. [CrossRef]

8. Czaja, W.; Krystynowicz, A.; Bielecki, S.; Brown, R.M., Jr. Microbial cellulose—The natural power to heal wounds. *Biomaterials* **2006**, *27*, 145–151. [CrossRef] [PubMed]

9. Klemm, D.; Schumann, D.; Udhardt, U.; Marsch, S. Bacterial synthesized cellulose—Artificial blood vessels for microsurgery. *Prog. Polym. Sci.* **2001**, *26*, 1561–1603. [CrossRef]

10. Wan, Y.; Gao, C.; Han, M.; Liang, H.; Ren, K.; Wang, Y.; Luo, H. Preparation and characterization of bacterial cellulose/heparin hybrid nanofiber for potential vascular tissue engineering scaffolds. *Polym. Adv. Technol.* **2011**, *22*, 2643–2648. [CrossRef]

11. Wang, J.; Gao, C.; Zhang, Y.; Wan, Y. Preparation and *in vitro* characterization of BC/PVA hydrogel composite for its potential use as artificial cornea biomaterial. *Mater. Sci. Eng. C Mater. Biol. Appl.* **2010**, *30*, 214–218. [CrossRef]

12. Trovatti, E.; Freire, C.S.R.; Pinto, P.C.; Almeida, I.F.; Costa, P.; Silvestre, A.J.D.; Neto, C.P.; Rosado, C. Bacterial cellulose membranes applied in topical and transdermal delivery of lidocaine hydrochloride and ibuprofen: *In vitro* diffusion studies. *Int. J. Pharm.* **2012**, *435*, 83–87. [CrossRef] [PubMed]

13. Müller, A.; Ni, Z.; Hessler, N.; Wersarg, F.; Müller, F.A.; Kralish, D.; Fisher, D. The biopolymer bacterial nanocellulose as drug delivery system: Investigation of drug loading and release using the model protein albumin. *J. Pharm. Sci.* **2013**, *102*, 579–592. [CrossRef] [PubMed]

14. Svensson, A.; Nicklasson, E.; Harrah, T.; Panilaitis, B.; Kaplan, D.L.; Brittberg, M.; Gatenholm, P. Bacterial cellulose as a potential scaffold for tissue engineering of cartilage. *Biomaterials* **2005**, *26*, 419–431. [CrossRef] [PubMed]

15. Angelova, N.; Hunkeler, D. Rationalizing the design of polymeric biomaterials. *Trends Biotechnol.* **1999**, *17*, 409–421. [CrossRef]

16. Bächdahl, H.; Helenius, G.; Bodin, A.; Nannmark, U.; Johansson, B.R.; Risberg, B.; Gatenholm, P. Mechanical properties of bacterial cellulose and interactions with smooth muscle cells. *Biomaterials* **2006**, *27*, 2141–2149. [CrossRef] [PubMed]

17. Barud, H.G.O.; Silva, R.R.; Barud, H.S.; Tercjak, A.; Gutierrez, J.; Lustri, W.R.; Ribeiro, S.J.L. A multipurpose natural and renewable polymer in medical applications: Bacterial cellulose. *Carbohydr. Polym.* **2016**, *153*, 406–420. [CrossRef] [PubMed]

18. Kwon, H.J.; Han, Y. Chondroitin sulfate-based biomaterials for tissue engineering. *Turkish J. Biol.* **2016**, *40*, 290–299. [CrossRef]

19. Campo, V.L.; Kawano, D.F.; da Silva, D.B., Jr.; Carvalho, I. Carrageenans: Biological properties, chemical modifications and structural analysis–A review. *Carbohydr. Polym.* **2009**, *77*, 167–180. [CrossRef]

20. Pereira, L.; Amado, A.M.; Critchley, A.T.; van de Velde, F.; Ribeiro-Claro, P.J.A. Identification of selected seaweed polysaccharides (phycocolloids) by vibrational spectroscopy (FTIR-ATR and FT-Raman). *Food Hydrocoll.* **2009**, *23*, 1903–1909. [CrossRef]

21. Necas, J.; Bartosikova, L. Carrageenan: A review. *Vet. Med.* **2013**, *58*, 187–205. [CrossRef]

22. Kong, L.; Ziegler, G.R. Fabrication of κ-carrageenan fibers by wet spinning: Spinning parameters. *Materials* **2011**, *4*, 1805–1817. [CrossRef] [PubMed]

23. Rhein-Knudsen, N.; Ale, M.T.; Meyer, A.S. Seaweed Hydrocolloid Production: An Update on Enzyme Assisted Extraction and Modification Technologies. *Mar. Drugs* **2015**, *13*, 3340–3359. [CrossRef] [PubMed]

24. Bornhöft, M.; Thommes, M.; Kleinebudde, P. Preliminary assessment of carrageenan as excipient for extrusion/spheronisation. *Eur. J. Pharm. Biopharm.* **2005**, *59*, 127–131. [CrossRef] [PubMed]

25. Ghanam, D.; Kleinbudde, P. Suitability of κ-carrageenan pellets for the formulation of multiparticulate tablets with modified release. *Int. J. Pharm.* **2011**, *409*, 9–18. [CrossRef] [PubMed]

26. Rocha, P.M.; Santo, V.E.; Gomes, M.E.; Reis, L.R.; Mano, J.F. Encapsulation of adipose-derived stem cells and transforming growth factor-β1 in carrageenan-based hydrogels for cartilage tissue engineering. *J. Bioact. Compat. Polym.* **2011**, *26*, 493–507. [CrossRef]

27. Boateng, J.S.; Pawar, H.V.; Tetteh, J. Polyox and carrageenan based composite film dressing containing anti-microbial and anti-inflammatory drugs for effective wound healing. *Int. J. Pharm.* **2013**, *441*, 181–191. [CrossRef] [PubMed]

28. Mihaila, S.M.; Gaharwar, A.K.; Reis, R.L.; Marques, A.P.; Gomes, M.E.; Khademhosseini, A. Photocrosslinkable kappa-carrageenan hydrogels for tissue engineering applications. *Adv. Healthc. Mater.* **2013**, *2*, 895–907. [CrossRef] [PubMed]

29. Newton, P.T.; Staines, K.A.; Spevak, L.; Boskey, A.L.; Teixeira, C.C.; Macrae, V.E.; Canfield, A.E.; Farguharson, C. Chondrogenic ATDC5 cells: An optimized model for rapid and physiological matrix mineralization. *Int. J. Mol. Med.* **2012**, *30*, 1187–1193. [CrossRef] [PubMed]

30. Park, S.; Baker, J.O.; Himmel, M.E.; Parilla, P.A.; Johnson, D.K. Cellulose crystallinity index: Measurement techniques and their impact on interpreting cellulose performance. *Biotechnol. Biofuels* **2010**, *3*, 3–10. [CrossRef] [PubMed]

31. Rabiej, M. A hybrid immune-evolutionary strategy algorithm for the analysis of the wide-angle X-ray diffraction curves of semicrystalline polymers. *J. Appl. Crystallogr.* **2014**, *47*, 1502–1511. [CrossRef]

32. Schrecker, S.T.; Gostomski, P.A. Determining the water holding capacity of microbial cellulose. *Biotechnol. Lett.* **2005**, *27*, 1435–1438. [CrossRef] [PubMed]

33. Shezad, O.; Khan, S.; Khan, T.; Park, J.K. Physicochemical and mechanical characterization of bacterial cellulose produced with an excellent productivity in static conditions using a simple fed-batch cultivation strategy. *Carbohydr. Polym.* **2010**, *82*, 173–180. [CrossRef]

34. Livak, K.J.; Schmittgen, T.D. Analysis of relative gene expression data using real-time quantitative PCR and the $2^{-\Delta\Delta C_T}$ method. *Methods* **2001**, *25*, 402–408. [CrossRef] [PubMed]

35. Saibuatong, O.-A.; Phisalaphong, M. Novo aloe vera-bacterial cellulose composite film from biosynthesis. *Carbohydr. Polym.* **2010**, *79*, 455–460. [CrossRef]

36. Hirai, A.; Tsuji, M.; Yamamoto, H.; Horii, F. *In situ* crystallization of bacterial cellulose III. Influences of different polymeric additives on the formation of microfibrils as revealed by transmission electron microscopy. *Cellulose* **1998**, *5*, 201–213. [CrossRef]

37. Shibazaki, H.; Saito, M.; Kuga, S.; Okano, T. Native cellulose II production by *Acetobacter xylinum* under physical constraints. *Cellulose* **1998**, *5*, 165–173. [CrossRef]

38. Kim, J.; Cai, Z.; Lee, H.S.; Choi, G.S.; Lee, D.H.; Jo, C. Preparation and characterization of a bacterial cellulose/chitosan composite for potential biomedical application. *J. Polym. Res.* **2011**, *18*, 739–744. [CrossRef]

39. Rahman, M.R.A.; Muhamad, I.I.; Hidayah, S.N.; Pa'e, N. Characterization of bacterial cellulose-chitosan composite membrane grafted with theophylline-imprinted copolymer. *Appl. Polym. Sci.* **2013**, *1*, 167–187.

40. Barud, H.S.; de Araújo Junior, A.M.; Santos, D.B.; de Assunção, R.M.N.; Meireles, C.S.; Cerqueira, D.A.; Filho, G.R.; Ribeiro, C.A.; Messaddeq, Y.; Ribeiro, S.J.L. Thermal behavior of cellulose acetate produced from homogeneous acetylation of bacterial cellulose. *Thermochim. Acta* **2008**, *471*, 61–69. [CrossRef]

41. Kačuráková, M.; Smith, A.C.; Gidley, M.J.; Wilson, R.H. Molecular interactions in bacterial cellulose composites studied by 1D FT-IR and dynamic 2D FT-IR spectroscopy. *Carbohydr. Res.* **2002**, *337*, 1145–1153. [CrossRef]

42. Gómez-Ordóñez, E.; Rupérez, P. FTIR-ATR spectroscopy as a tool for polysaccharide identification in edible brown and red seaweeds. *Food Hydrocoll.* **2011**, *25*, 1514–1520. [CrossRef]

43. Devi, N.; Maji, T.K. A novel microencapsulation of neem (Azadirachta indica A. Juss.) seed oil (NSO) in polyelectrolyte complex of κ-carrageenan and chitosan. *J. Appl. Polym. Sci.* **2009**, *113*, 1576–1583. [CrossRef]

44. Zhou, L.L.; Sun, D.P.; Hu, L.Y.; Li, Y.W.; Yang, J.Z. Effect of addition of sodium alginate on bacterial cellulose production by *Acetobacter xylinum*. *J. Ind. Microbiol. Biotechnol.* **2007**, *34*, 483–489. [CrossRef] [PubMed]

45. Awadhiya, A.; Kumar, D.; Rathore, K.; Fatma, B.; Verma, V. Synthesis and characterization of agarose-bacterial cellulose biodegradable composites. *Polym. Bull.* **2017**, *74*, 2887–2903. [CrossRef]

46. Jia, Y.; Wang, X.; Huo, M.; Zhai, X.; Li, F.; Zhong, C. Preparation and characterization of a novel bacterial cellulose/chitosan bio-hydrogel. *Nanomater. Nanotechnol.* **2017**, *7*, 1–8. [CrossRef]

47. Yang, Q.; Ma, H.; Dai, Z.; Wang, J.; Dong, S.; Shen, J.; Dong, J. Improved thermal and mechanical properties of bacterial cellulose with the introduction of collagen. *Cellulose* **2017**, *24*, 3777–3787. [CrossRef]

48. Sya'di, Y.K.; Wahyuni, E.T.; Rahayu, E.S.; Cahyanto, M.N. The effect of polysaccharide in the fermentation medium on physical properties of bacterial cellulose form *Gluconacetobacter xylinus* BTCC B796. *Pak. J. Biotechnol.* **2017**, *3*, 323–327.

49. Paximada, P.; Dimitrakopoulou, E.A.; Tsouko, E.; Koutinas, A.A.; Fasseas, C.; Mandala, I.G. Structural modification of bacterial cellulose fibrils under ultrasonic irradiation. *Carbohydr. Polym.* **2016**, *150*, 5–12. [CrossRef] [PubMed]

50. Ciechańska, D. Multifunctional bacterial cellulose/chitosan composite materials for medical applications. *Fibres Text. East. Eur.* **2004**, *12*, 69–72. [CrossRef]

51. Ul-Islam, M.; Khan, T.; Park, J. Water holding and release properties of bacterial cellulose obtained by *in situ* and *ex situ* modification. *Carbohydr. Polym.* **2012**, *88*, 596–603. [CrossRef]

52. Hezaveh, H.; Muhamad, I.I. Modification and swelling kinetic study of kappa-carrageenan-based hydrogel for controlled release study. *J. Taiwan Inst. Chem. Eng.* **2013**, *44*, 182–191. [CrossRef]

53. Klemm, D.; Kramer, F.; Moritz, S.; Lindström, T.; Ankerfors, M.; Gray, D.; Dorri, A. Nanocelluloses: A new family of nature-based materials. *Angew. Chem. Int. Ed.* **2011**, *50*, 5438–5466. [CrossRef] [PubMed]

54. Lacroix, D.; Prendergast, P.J. A mechano-regulation model for tissue differentiation during fracture healing: Analysis of gap size and loading. *J. Biomech.* **2002**, *35*, 1163–1171. [CrossRef]

55. Eleswarapu, S.V.; Responte, D.J.; Athanasiou, K.A. Tensile properties, collagen content, and crosslinks in connective tissues of the immature knee joint. *PLoS ONE* **2011**, *6*, e26178. [CrossRef] [PubMed]

56. Toyoda, T.; Seedhom, B.B.; Yao, J.Q.; Kirkham, J.; Brookes, S.; Bonass, W.A. Hydrostatic pressure modulates proteoglycan metabolism in chondrocytes seeded in agarose. *Arthritis Rheum.* **2003**, *48*, 2865–2872. [CrossRef] [PubMed]

57. Elder, B.D.; Athanasiou, A.K. Hydrostatic pressure in articular cartilage tissue engineering: From chondrocytes to tissue regeneration. *Tissue Eng. Part B Rev.* **2009**, *15*, 43–53. [CrossRef] [PubMed]

58. Favi, P.M.; Benson, R.S.; Neilsen, N.R.; Hammonds, R.L.; Bates, C.C.; Stephens, C.P.; Dhar, M.S. Cell proliferation, viability, and *in vitro* differentiation of equine mesenchymal stem cells seeded on bacterial cellulose hydrogel scaffolds. *Mater. Sci. Eng.* **2013**, *33*, 1935–1944. [CrossRef] [PubMed]

59. Sathuvan, M.; Thangam, R.; Gajendiran, M.; Vivek, R.; Balasubramanin, S.; Nagaraj, S.; Gunasekaran, P.; Madhan, B.; Rengasamy, R. κ-Carrageenan: An effective drug carrier to deliver curcumin in cancer cells and to induce apoptosis. *Carbohydr. Polym.* **2017**, *169*, 184–193. [CrossRef] [PubMed]

60. Ma, B.; Leijten, J.C.H.; Wu, L.; Kip, M.; van Blitterswijk, C.A.; Post, J.N.; Karperien, M. Gene expression profiling of dedifferentiated human articular chondrocytes in monolayer culture. *Osteoarthr. Cartil.* **2013**, *21*, 599–603. [CrossRef] [PubMed]

61. Hata, K.; Takahata, Y.; Murakami, T.; Nishimura, R. Transcriptional Network Controlling Endochondral Ossification. *J. Bone Metab.* **2017**, *24*, 75–82. [CrossRef] [PubMed]

62. Demoor, M.; Ollitrault, D.; Gomez-Leduc, T.; Bouyoucef, M.; Hervieu, M.; Fabre, H.; Lafont, J.; Denoix, J.-M.; Audigié, F.; Mallein-Gerin, F.; et al. Cartilage tissue engineering: Molecular control of chondrocyte differentiation for proper cartilage matrix reconstruction. *Biochim. Biophys. Acta* **2014**, *1840*, 2414–2440. [CrossRef] [PubMed]

63. Vinatier, C.; Gauthier, O.; Fatimi, A.; Merceron, C.; Masson, M.; Moreau, A.; Moreau, F.; Fellah, B.; Weiss, P.; Guicheux, J. An injectable cellulose-based hydrogel for the transfer of autologous nasal chondrocytes in articular defects. *Biotechnol. Bioeng.* **2009**, *102*, 1259–1267. [CrossRef] [PubMed]

64. Kwon, H.J.; Yasud, K.; Ohmiya, Y.; Honma, K.; Chen, Y.M.; Gong, J.P. *In vitro* differentiation of chondrogenic ATDC5 cells is enhanced by culturing on synthetic hydrogels with various charge densities. *Acta Biomater.* **2010**, *6*, 494–501. [CrossRef] [PubMed]